Journal of Materials Chemistry C

PAPER

View Article Online
View Journal

Cite this: DOI: 10.1039/c9tc03548f

Origin of dual emission in σ-bridged donor–acceptor TADF compounds†

Rokas Skaisgiris, [a] Tomas Serevičius, *[a] Karolis Kazlauskas, [a] Yan Geng,[b] Chihaya Adachi *[cd] and Saulius Juršėnas[a]

Received 1st July 2019,
Accepted 20th September 2019

DOI: 10.1039/c9tc03548f

rsc.li/materials-c

The desire to boost the reverse intersystem crossing rate and obtain thermally activated delayed fluorescence with sub-microsecond lifetime fosters the search for novel concepts of molecular geometry. Recently, TADF compounds made of acridine, tetramethylcarbazole and triphenylamine donor and triphenyltriazine acceptor units bound by hyperconjugated spacer units were introduced as having very rapid double TADF decay. Here we present an in-depth time-resolved fluorescence analysis of these intriguing donor–σ–acceptor TADF compounds in various surroundings. Extremely weak coupling of electron-donating and electron-accepting units was found for the σ-bridged TADF compounds, resulting in the coexistence of intramolecular and exciplex fluorescence, whose interplay allowed one to tune the emission properties. The initial fluorescence decay in toluene solutions, previously attributed to rapid TADF, was shown to be prompt intramolecular fluorescence with prolonged fluorescence lifetime, susceptible to molecular oxygen. Only the later delayed fluorescence at the microsecond time-scale, originating from the exciplex states, was attributed to TADF. On the contrary, dominant intramolecular TADF was observed in dilute PMMA films with weaker non-radiative decay. The smooth transition from intramolecular to exciplex TADF was observed by increasing the doping concentration of the polymer films. The DF/PF ratio was found to increase with increasing doping concentration due to the emergence of additional exciplex TADF until a 20 wt% doping load, where concentration quenching emerged at larger doping ratios. The presented findings showcase the unusual fluorescence properties of TADF compounds with weakly bound donor and acceptor units and are important for the future design of novel TADF compounds.

Introduction

Organic light emitting diodes (OLEDs) are highly attractive for lighting and display applications due to their unmatched contrast ratio, lightness and flexibility. The long history of OLED science, dating back to the report by Tang and Van Slyke,[1] mostly was devoted to the improvement of the external quantum efficiency (EQE), which was limited by the dark triplet states. The singlet exciton yield of electrically injected charge carriers for 1st generation fluorescent OLEDs is only 25%, limiting their external quantum efficiency (EQE) to up to about 5%. Later, a new class of phosphorescent emitters employing the internal heavy atom effect was introduced.[2] The involvement of heavy rare-earth atoms, *e.g.*, iridium, resulted in the remarkable enhancement of the spin–orbit coupling, converting all excitons to short-lived triplet ones. This strategy allowed one to reach 100% internal quantum efficiency (IQE) and an EQE of 20% for phosphorescent OLEDs.[3] However, phosphorescent compounds, especially blue emitters, suffer from instability. Moreover, the requirement of rare-earth metals increased the cost of devices and raised concerns over their toxicity. The stability and high-cost issues were solved by introducing 3rd generation all-organic emitters employing thermally activated delayed fluorescence.[4,5] In this case, molecular compounds are designed to have small singlet–triplet energy splitting (ΔE_{ST}), where the triplet excitons are thermally assisted to perform reverse intersystem crossing with internal quantum efficiencies up to 100%.[6,7] Several different approaches for the realization of small ΔE_{ST} were suggested: minimization of the exchange interaction by using donor–acceptor molecular compounds,[5] utilization of multiple resonance effects[8] or by employing the excited-states.[9,10] Yet, the donor–acceptor core still is the mostly used TADF design. In this case efficient reverse

[a] Institute of Photonics and Nanotechnology, Vilnius University, Sauletekio 3, LT-10257, Vilnius, Lithuania. E-mail: tomas.serevicius@tmi.vu.lt
[b] College of Chemistry, Chemical Engineering and Materials Science, Collaborative Innovation Center of Functionalized Probes for Chemical Imaging in Universities of Shandong, Key Laboratory of Molecular and Nano Probes, Ministry of Education, Shandong Normal University, Jinan 250014, P. R. China
[c] Center for Organic Photonics and Electronics Research (OPERA), and International Institute for Carbon Neutral Energy Research (WPI-I²CNER), Kyushu University, Fukuoka 819-0395, Japan. E-mail: adachi@cstf.kyushu-u.ac.jp
[d] Japan Science and Technology Agency ERATO, Adachi Molecular Exciton Engineering Project, Fukuoka 819-0395, Japan

† Electronic supplementary information (ESI) available. See DOI: 10.1039/c9tc03548f

intersystem crossing (rISC) is achieved by minimizing the exchange energy, which is directly proportional to the HOMO–LUMO overlap,[11] and ensuring strong vibronic coupling between the localized (^{3}LE) and charge-transfer (^{3}CT) triplet states.[12,13] Small HOMO–LUMO overlap is attained in compounds constructed of electron-donating (D) and electron-accepting (A) molecular fragments with balanced steric hindrance, having pronounced charge-transfer (CT) character and non-negligible radiative recombination rates.

The same concept based on the minimization of ΔE_{ST} by reducing the HOMO–LUMO overlap was utilized in exciplex emitters,[14,15] composed of electron-donating and electron-accepting molecular materials. Though small ΔE_{ST} in exciplex systems can be realized more easily due to the intermolecular nature of charge transfer and rather efficient exciplex-based OLEDs with EQEs approaching 20% have been presented,[16] the efficiency of exciplex TADF strongly depends on the distance between the donor and acceptor fragments,[17] which is difficult to control. This strongly complicates the applications of exciplex TADF OLEDs. To overcome the shortcomings of exciplex TADF, a novel strategy was suggested. In this case the donor and acceptor units were bound in close proximity (*e.g.* several Å) with conjugated[18] or non-conjugated[19–22] spacers utilizing intermolecular through-space charge transfer. Rather efficient exciplex TADF can be achieved with fluorescence quantum efficiencies (Φ_F) up to about 60% and EQEs up to about 12%. Another promising pathway for similar ''fixed'' exciplex systems is to employ hyperconjugation,[23,24] which allows one to bind two separated π-conjugated electron systems. Recently, we have suggested a novel donor–σ–acceptor geometry utilizing the hyperconjugation effect to obtain TADF.[25] Several donor units were bound to a triphenyltriazine acceptor fragment by a hexafluoroisopropylidene spacer unit. In this case, the hyperconjugation between the donor and acceptor moieties ensured very small HOMO–LUMO overlap and ΔE_{ST} together with the intramolecular nature of CT. The DFT-estimated oscillator strengths were very low (in the range of 0.0008–0.0054), typical for weakly interacting donor and acceptor systems. Dual TADF decay was observed, one of which was very rapid with a lifetime of only 200–400 ns, which is one of the shortest ever reported.[26] Successful realization of TADF with sub-microsecond lifetime in similar hyperconjugation-based compounds could open new possibilities for realization of highly efficient OLEDs with low roll-off.[27]

Inspired by the intriguing TADF properties of donor–σ–acceptor TADF compounds with sub-microsecond lifetime,[25] here we performed a comprehensive time-resolved fluorescence study of σ-bridged TADF compounds with dual upconversion in various surroundings. The analysis of viscosity, concentration and temperature-dependent fluorescence spectra of the TADF compounds in dilute solutions, and dilute polymer and neat films revealed the interplay of two different CT states, decaying on different time-scales. The molecular concentration and ambient viscosity were shown to tune the emission type, intramolecular or intermolecular CT or even from both types simultaneously. Intramolecular TADF was observed only in dilute polymer films, while the coexisting exciplex emission was shown to be of TADF nature in solutions and films at high doping concentration.

Experimental details

The photophysical properties were measured in 1.2×10^{-5} M toluene solutions, PMMA (poly(methylmethacrylate)) films with variable doping concentration (1–100 wt%) and neat films. The analysis of the CT state was also performed in 1×10^{-4} M toluene solutions. The PMMA films were prepared by dissolving the compound and PMMA at appropriate ratios in toluene and then drop-casting at room temperature on a quartz substrate. The neat films were prepared from 5 mg ml^{-1} toluene solution by spin-coating at 800 rpm for 1 min and finalizing with 8 min of 4000 rpm to accelerate the evaporation of toluene. To modify the viscosity of toluene, PMMA polymer was added into the solution in different proportions.[28] The absorption spectra were measured using a UV-vis-NIR spectrophotometer Lambda 950 (PerkinElmer). Steady-state emission spectra were recorded using a CCD spectrometer PMA-11 (Hamamatsu) coupled with a CW xenon lamp (FWHM $<$ 10 nm). Fluorescence quantum yields (Φ_F) were obtained by using the integrating sphere method.[29] Time-resolved fluorescence spectra, fluorescence decay transients and phosphorescence spectra were obtained by using a nanosecond YAG:Nd^{3+} laser NT 242 with an optical parametric generator (Ekspla, excitation wavelength 300 nm, pulse duration 7 ns, repetition rate 1 kHz, 50 nJ per pulse fluence) and time-gated intensified CCD camera iStar DH340T (Andor) with a spectrograph SR-303i (Shamrock). Phosphorescence spectra were measured at a 10 K temperature after a 100 μs delay with a 890 μs integration time. Fluorescence decay transient measurements were performed by exponentially increasing the delay and integration time as described in ref. 30. This allowed us to record up to 10 orders of magnitude in time and intensity of the photoluminescence decay. Five repetitive freeze–pump–thaw cycles were used to deoxygenate the toluene solutions. The polymer samples were mounted in a closed cycle He cryostat (Cryo Industries 204N) for both oxygen-saturated and oxygen-free (at a 1×10^{-4} Torr pressure) measurements. Temperature dependent measurements were performed in the same closed cycle He cryostat.

Results and discussion

Materials and steady-state spectroscopy analysis of dilute solutions

Three TADF compounds of donor–σ–acceptor structure were analyzed (see Fig. 1). A planar triphenyltriazine fragment was used as an electron-acceptor unit while dihydroacridine (**1**), tetramethylcarbazole (**2**) and triphenylamine (**3**) were selected as electron-donating units with different electron-donating strengths.[31] Hexafluoroisopropylidene was used as a σ-spacer. Synthetic details, initial DFT calculations and a brief analysis of the fluorescence properties were reported elsewhere[25] and are

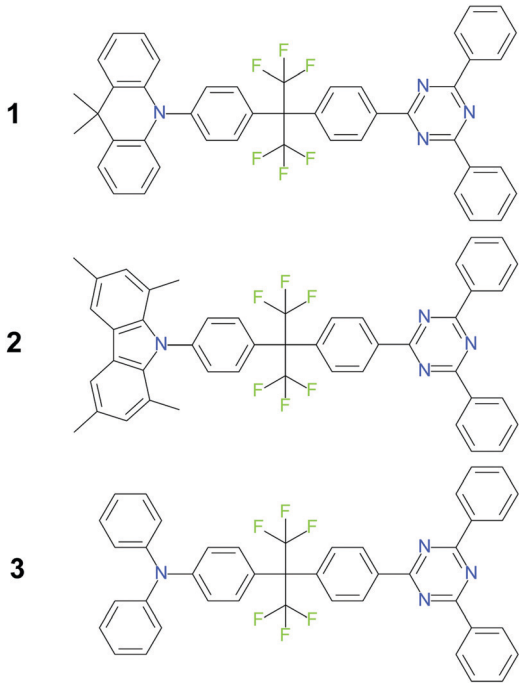

Fig. 1 Chemical structures of donor–σ–acceptor compounds **1–3**.

briefly reported in this chapter, while thorough spectroscopic analysis will be presented in the following chapters.

The absorption spectra peaked below 300 nm with weak absorption of intramolecular charge transfer (ICT) origin at about 300–370 nm, observed for all compounds, in-line with the DFT predictions.[25] Negligible oscillator strengths of 0.0008, 0.0012 and 0.0054 were simulated for compounds **1–3**, respectively. The fluorescence spectra of toluene solutions peaked in the range of 437–463 nm. The broad and structureless spectral lineshape indicated the charge-transfer nature. Locally excited (^{1}LE) state emission at about 360 nm was clearly observed for compound **2**, originating from the tetramethylcarbazole donor unit,[25] while for the rest of the compounds the ^{1}LE intensity was lower. The low-temperature phosphorescence spectra of toluene solutions (LTPh) were of ^{3}LE nature with the lowest energy vibronic replicas peaking at 415–419 nm. Singlet–triplet energy gaps (ΔE_{ST}) of 0.06, 0.07 and 0.18 eV were estimated for compounds **1**, **2** and **3**, respectively.[25]

Excited state relaxation in dilute solutions

The fluorescence decay transients of donor–σ–acceptor compounds **1–3** at the CT emission peak in oxygen-free ($-O_2$) toluene followed a double-exponential decay (see Fig. 2). Initially, the fluorescence decayed with a lifetime of 37–470 ns (τ_{FL1}), followed by later slower decay with a lifetime (τ_{FL2}) of 0.45–10 μs (see Table 1 for details). The presence of oxygen strongly quenched both CT fluorescence bands. Both fluorescence decays in $-O_2$ toluene, the fast and the slower one, were attributed to TADF in the initial analysis.[25] Fluorescence quenching by oxygen and TADF intensity activation with temperature were used as the proof. However, the nature of both decays is more complex.

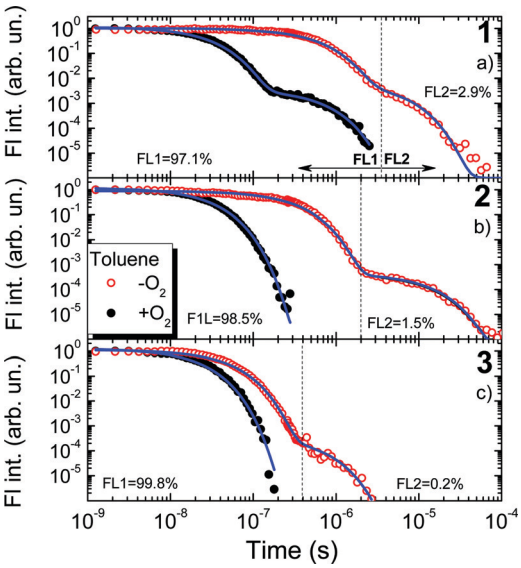

Fig. 2 Normalized fluorescence decay transients of donor–σ–acceptor compounds **1** (a), **2** (b) and **3** (c) in oxygen-saturated ($+O_2$) and oxygen-free ($-O_2$) toluene solutions. Fractional intensities of the initial and delayed fluorescence in $-O_2$ conditions are also noted.

Table 1 Fluorescence data of donor–σ–acceptor compounds **1–3** in oxygen-free toluene

	τ_{FL}[a] (ns)	τ_{TADF}[b] (μs)	DF/PF[c]
1	470	4.5	0.03
2	250	10	0.015
3	37	0.45	0.002

[a] Fluorescence decay time of the initial fluorescence. [b] Fluorescence decay time of the delayed fluorescence. [c] Time-integrated delayed and prompt fluorescence intensity ratio.

The initial decay with a lifetime of 37–470 ns could also be prompt fluorescence. This would not be surprising for weakly coupled D–σ–A compounds with small HOMO–LUMO overlap and negligible oscillator strengths. The lowest oscillator strength was estimated for compound **1** with the largest τ_{FL1} while the lowest τ_{FL1} was for compound **3** with the largest oscillator strength. ΔE_{ST} and the TADF lifetime also depend on the HOMO–LUMO overlap[11] (and thus the oscillator strength) and more rapid TADF decay should be observed for compounds with smaller ΔE_{ST}. The smallest singlet–triplet energy gap was estimated for compounds **1** and **2** (60 and 70 meV, respectively), while for compound **3** it was remarkably larger (180 meV). However, the opposite trend was observed. As we can see, τ_{FL1} was the longest for the compound with the lowest ΔE_{ST} and it was the shortest for the compound with the largest ΔE_{ST}. Such a trend is the opposite of what we would expect for TADF, but in-line with the trend for prompt fluorescence: the longest τ_{FL1} was observed for compound **1** with the strongest dihydroacridine donor unit[25,31] and the lowest oscillator strength, while the shortest τ_{FL1} was observed for compound **3** with the weakest triphenylamine donor unit and the largest oscillator strength. This prompt fluorescence was shown to be susceptible to molecular oxygen. This is rather unusual, however singlet states

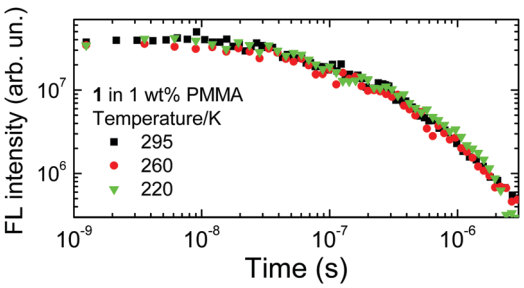

Fig. 3 Initial fluorescence decay transients of 1 wt% PMMA films of compounds **1–3**.

have been shown to be sensitive to molecular oxygen.[32–34] Our donor–σ–acceptor compounds with especially long prompt fluorescence lifetime could be even more prone to quenching by molecular oxygen.

To analyze the nature of the initial fluorescence, temperature-dependent measurements of fluorescence transients were performed in dilute toluene (see Fig. S6 and S7 in ref. 25) and the decrease of τ_{FL1} was observed at larger temperatures, typical for TADF. However, when the compounds were embedded into PMMA polymer films (see Fig. 3), the lifetime and the intensity of the initial decay were insensitive to the temperature. Toluene has a melting point of 178 K, therefore it remained in the liquid state in the temperature range of 300–200 K, thus the variation of the non-radiative recombination rate upon the temperature decrease was not neglected. The impact of non-radiative decay was strongly suppressed in the rigid polymer film, where no thermal activation was observed, typical for prompt fluorescence.

The decay time of the later fluorescence, observed at the microsecond time-scale, was 4.5, 10 and 0.45 μs (an approximate value due to the low emission intensity) for compounds **1**, **2** and **3**, respectively. In this case, the second decay component followed TADF-like behavior: its lifetime was lower for compounds with lower ΔE_{ST} and the DF/PF ratio was larger for compounds with lower ΔE_{ST} (see Table 1).

To conclude, the initial fluorescence decay could hardly be attributed to TADF. The experimental evidence shows its non-TADF nature. Only the later fluorescence, observed at the microsecond time-scale, can be attributed to TADF.

Two charge-transfer states in dilute solutions

The time-integrated fluorescence spectra (TIFL) of compounds **1–3** in toluene[25] showed only one dominating CT fluorescence band with a double-exponential decay profile. On the contrary, time-resolved fluorescence spectra (TRFL) analysis (see Fig. 4) revealed the presence of more complex structure of the emission spectra. Two CT fluorescence spectra were observed at different time-scales. Initially, the first CT fluorescence band ($^1CT_1$) was observed at about 445–465 nm up to about 4 μs, 2 μs and 0.5 μs for compounds **1–3**, respectively. At later delays, the second CT fluorescence band ($^1CT_2$) clearly emerged, peaking at about 475–505 nm (see Fig. S1 in the ESI†). Some long-wavelength shoulders of the fluorescence spectra, extending up to 600–650 nm, were observed for all compounds even at the smallest

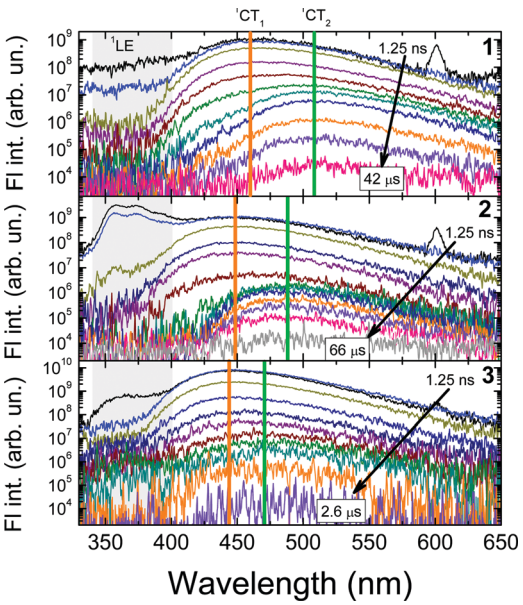

Fig. 4 Time-resolved fluorescence spectra of donor–σ–acceptor compounds **1–3** in oxygen-free toluene at 1.2×10^{-5} M concentration. The numbers in the picture denote the initial and final delay times.

delay times, showing that the weak second CT state probably is formed after the photoexcitation, but is overwhelmed by fluorescence of the $^1CT_1$ state. The $^1CT_2$ emission was more susceptible to oxygen quenching than that of the $^1CT_1$ states (see Fig. S2 in the ESI†). Since the prompt and delayed fluorescence are observed at different wavelengths, the true TADF transients at larger delays are those obtained at the $^1CT_2$ peak (see Fig. S3 in the ESI†). An enhanced TADF intensity was observed (up to about 5–6 times) with the same lifetime.

The nature of both CT states needs further analysis. Clearly, both emission bands are of CT-nature and their peak energies depend on the strength of the donor unit: the stronger the donor, the more redshifted the emission wavelength. The energy difference between the CT bands was 240, 220 and 160 meV for compounds **1–3**, respectively. The second emission band, which becomes clearly evident only at later delays, could originate from, *e.g.*, dynamic molecular conformer states, emerging after the reorganization of the molecular structure,[35] or exciplex states,[36] formed between the donor and acceptor units from separate molecules after diffusion at long time-scales.

To test the nature of the second CT state, the fluorescence decay transients of compound **1** were measured in $-O_2$ toluene solutions with adjustable viscosity (see Fig. 5 and the Experimental section for details). More viscous toluene surrounding had a weak effect on the prompt emission, slightly decreasing its decay time from 470 to 280 ns, while the increased viscosity strongly quenched the TADF, where the DF/PF ratio decreased from 0.15 to 0.003 (see Table 2). The decrease of the prompt fluorescence lifetime could be related with the changes of the non-radiative decay rate. It is clear that the TADF intensity is weakened in viscous surroundings, however still it is not clear whether the quenching of delayed emission was due to the impeded reorganization of the molecular structure or slowed

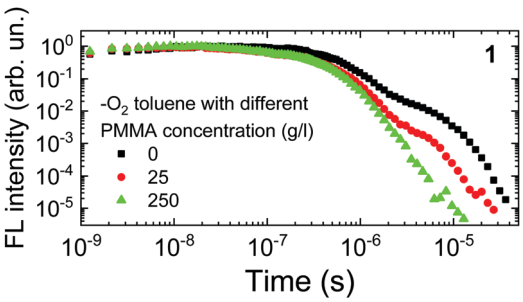

Fig. 5 Normalized fluorescence decay transients of compound **1** at the $^1CT_2$ peak in oxygen-free toluene solutions with different viscosity. The solution viscosity was varied by increasing the PMMA concentration.[28]

Table 2 Photoluminescence decay constants of compound **1** at the $^1CT_2$ peak in toluene with different viscosity

PMMA concentration[a] (g l^{-1})	DF/PF ratio[b]	$\tau_{^1CT_1}$[c] (ns)	$\tau_{^1CT_2}$[d] (μs)
0	0.18	470	4.5
25	0.03	320	2.8
250	0.003	280	1.25

[a] PMMA polymer concentration in oxygen-free toluene. [b] Intensity ratio between the time-integrated delayed and prompt fluorescence spectra. [c] Fluorescence decay time of the CT_1 state (prompt fluorescence). [d] Fluorescence decay time of the CT_2 state (TADF).

molecular diffusion and thus the lower contribution from exciplex states.

The presence of exciplex states was revealed by comparing the TADF properties of 1.2×10^{-5} and 1×10^{-4} M toluene solutions of compound **1** (see Fig. 6). The lineshape of the fluorescence spectra clearly was concentration dependent (see Fig. 6a), where the emission peak was redshifted from 475 nm to 485 nm upon the concentration increase. As we know from the analysis of the time-resolved fluorescence spectra (see Fig. 4), the time-integrated emission spectrum is formed of two distinct

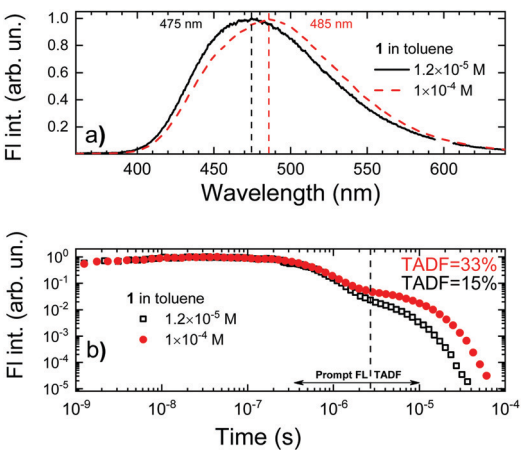

Fig. 6 (a) Normalized time-integrated fluorescence spectra of compound **1** in 1.2×10^{-5} M (solid line) and 10^{-4} M (dashed line) oxygen-free toluene solutions. (b) Fluorescence decay transients of compound **1** in 1.2×10^{-5} M (open symbols) and 10^{-4} M (closed symbols) oxygen-free toluene solutions at the $^1CT_2$ peak.

fluorescence bands of CT_1 and CT_2 states, peaking at about 465 nm and 505 nm (for compound **1**). Increasing the concentration of compound **1** in toluene clearly enhances the emission intensity from the $^1CT_2$ states and, therefore, shifts the peak of the total emission spectrum to longer wavelengths. A similar trend was observed for the fluorescence decay transients, obtained at the $^1CT_2$ emission peak (see Fig. 6b). Here we can see that the increased concentration of compound **1** in toluene solutions enlarged the intensity of the later decay part, attributed to exciplex TADF, increasing the DF/PF ratio from 0.18 to 0.49.

Clearly, viscosity and concentration-dependent measurements of fluorescence spectra support the prediction that the second CT state is of exciplex nature. It may look quite unusual to observe exciplex emission in solutions with concentrations as low as 1×10^{-5} M, however exciplex emission can be successfully observed in various dilute solutions of molecular compounds, especially for those containing large and planar units,[37–40] as in our σ-bonded D–A compounds. Additionally, exceptionally slow fluorescence decay should be beneficial for the observation of exciplex emission in solutions, when the probability of two molecules to meet each other before recombination is greatly enhanced. Obviously, the most intense intermolecular TADF was observed for the compound with the longest intramolecular fluorescence lifetime (see Fig. 2).

Suppression of the exciplex states in polymer films

For the further analysis of exciplex formation, compounds **1–3** were incorporated into a rigid PMMA polymer matrix at low concentration. In this case, emission should originate only from isolated molecules, since molecular diffusion is strongly impeded by the rigid polymer surroundings. The time-integrated fluorescence spectra of 1 wt% PMMA films of compounds **1–3** are shown in Fig. 7a. The emission spectra were very similar to those of the dilute solutions, showing dominating intramolecular CT emission peaking at 460, 455 and 445 nm for compounds **1–3**, respectively. Weak emission, related to the electron-donating unit, was clearly observed for compound **2**.

The fluorescence decay transients of 1 wt% PMMA films of compounds **1–3** are shown in Fig. 7b. The fluorescence decay followed the same trend as in toluene solutions, when two decay components were observed (see Fig. S4 in the ESI†). However, the fluorescence decay profiles were multiexponential, indicating the existence of conformational disorder, typical for TADF compounds.[41–44] Although the exact lifetime of the prompt and delayed emission could not be evaluated due to the multi-exponential nature, it is clear that the prompt fluorescence showed the same trend as in toluene solutions, where the slowest prompt fluorescence decay was observed for compound **1** and the most rapid for compound **3**. For the delayed emission, no clear trend was observed. The delayed fluorescence was quenched by oxygen (see Fig. S5 in the ESI†), typical for TADF. Temperature-dependent fluorescence decay transient measurements also supported our assumptions (see Fig. S6 in the ESI†). The intensity of the initial fluorescence and its lifetime were insensitive to temperature. On the other hand, the delayed emission showed temperature activation, typical for TADF. The TADF intensity was

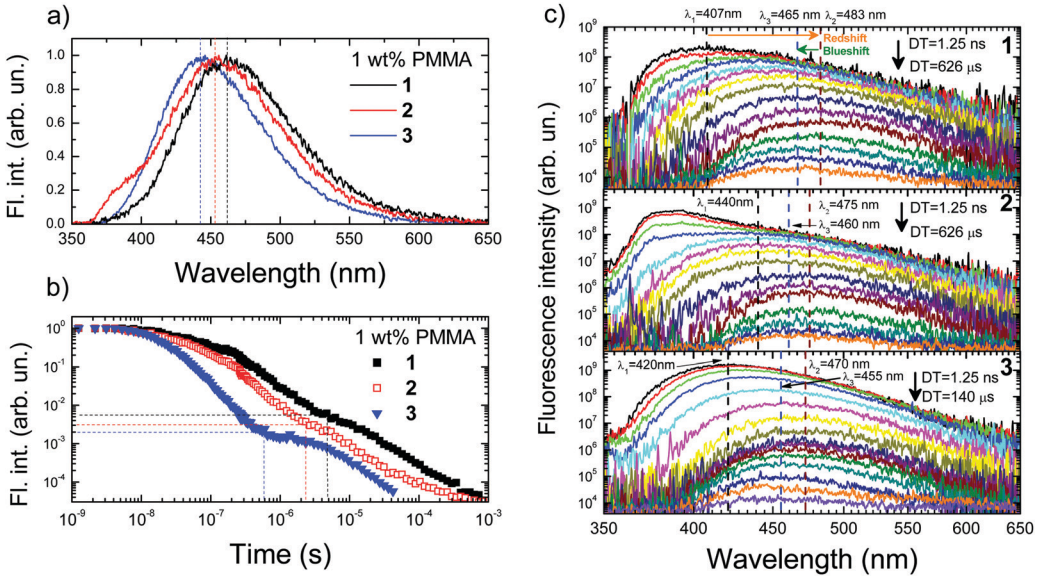

Fig. 7 (a) Normalized time-integrated fluorescence spectra of 1 wt% PMMA films of donor–σ–acceptor compounds **1–3**. Dashed lines are guides for the eye. (b) Normalized fluorescence decay transients of 1 wt% PMMA films of donor–σ–acceptor compounds **1–3** in $-O_2$ conditions. The dashed lines denote the initial intensity of the delayed emission and the delay time when the delayed emission emerges. (c) Time-resolved fluorescence spectra of 1 wt% PMMA films of donor–σ–acceptor compounds **1–3** in $-O_2$ conditions. DT denotes the initial and the latest delay times. λ_1, λ_2 and λ_3 represent the emission peak wavelengths of the initial, the most redshifted and the latest emission spectra, respectively.

remarkably enhanced in the polymer film, where the DF/PF ratios increased up to 1.08, 0.92 and 0.6 for compounds **1**, **2** and **3**, respectively. This was caused by the lowered non-radiative decay in more rigid surroundings and the presence of conformational disorder.[43]

The analysis of the time-resolved fluorescence spectra of compounds **1–3** embedded in 1 wt% PMMA films (see Fig. 7c) revealed the presence of temporal shifts of the emission peak due to the dispersion of ΔE_{ST}, typical for TADF in solid surroundings.[41–44] Initially, a redshift of the CT_1 state of about 210–480 meV was observed for about 0.5–4 μs, while at later delays a blueshift emerged. The blueshift was comparable for all compounds (~100 meV), while the lowest redshift was observed for compound **2** with the sterically-fixed tetramethylcarbazole donor unit. As it was expected, the $^1CT_2$ state was totally suppressed in the polymer films, again confirming its exciplex nature. Both fluorescence decay components, prompt and delayed, originated from the intramolecular $^1CT_1$ state. The non-radiative decay, especially through internal conversion, is remarkably weakened in the rigid polymer surroundings, allowing one to observe the delayed emission from the intramolecular states.

Exciplex states in neat films

In the final stage, the emission properties of neat films of donor–σ–acceptor compounds **1–3** were analyzed (see Fig. 8).

As we can see from Fig. 8a, the time-integrated fluorescence spectra of the neat films of compounds **1–3** were redshifted by about 140–190 meV compared to the 1 wt% PMMA films and by 180–200 meV compared to the 1.2×10^{-5} M toluene solutions and peaked at 495, 482 and 470 nm for compounds **1**, **2** and **3**, respectively. The redshift of the emission wavelength in neat films is a rather frequent effect for both fluorescent and TADF emitters[45,46] and usually occurs due to intermolecular interactions or solid state solvation. However, solid state solvation occurs with smaller magnitude due to the lower rotation ability of molecules and almost exclusively only after the inclusion of additional dopants with large ground-state dipole moments.[42,47,48] Usually the shift of the emission peak with increasing doping concentration occurs due to enhanced intermolecular interactions.[45,49] In our case, the TIFL spectra of the neat films of compounds **1–3** were found to coincide quite well with the fluorescence spectra of the $^1CT_2$ state from the toluene solutions (see the blue and green lines in Fig. 8a), attributed to the emission of exciplex states. The weak exciplex emission observed in toluene solution dominated in the neat films. This is not surprising, since the formation of excimer states should be enforced in the tightly-packed molecular environment of neat films.[24,50] The low-temperature phosphorescence spectra of compounds **1–3** were of different nature. If the LTPh spectra in toluene contained clear vibronic progressions, typical for ^3LE states (see Fig. 2 in ref. 25), the LTPh spectra of the neat films were structureless, indicating the intermolecular CT nature[24] (see Fig. S7 in the ESI†). A ΔE_{ST} of 60 and 90 meV was estimated for compounds **2** and **3**, respectively. Surprisingly, a negative ΔE_{ST} of −40 meV was estimated for **1**, probably due to the impact of the remaining phosphorescence from the intramolecular states.

The time-resolved fluorescence spectra of the neat films of compounds **1–3** are shown in Fig. S8 in the ESI.† The presence of conformational disorder was observed. Initially, the redshift of the emission spectra from about 460 nm to 490–510 nm was observed. No subsequent blueshift of the emission peak was noticed, probably due to the quenching of the latest delayed

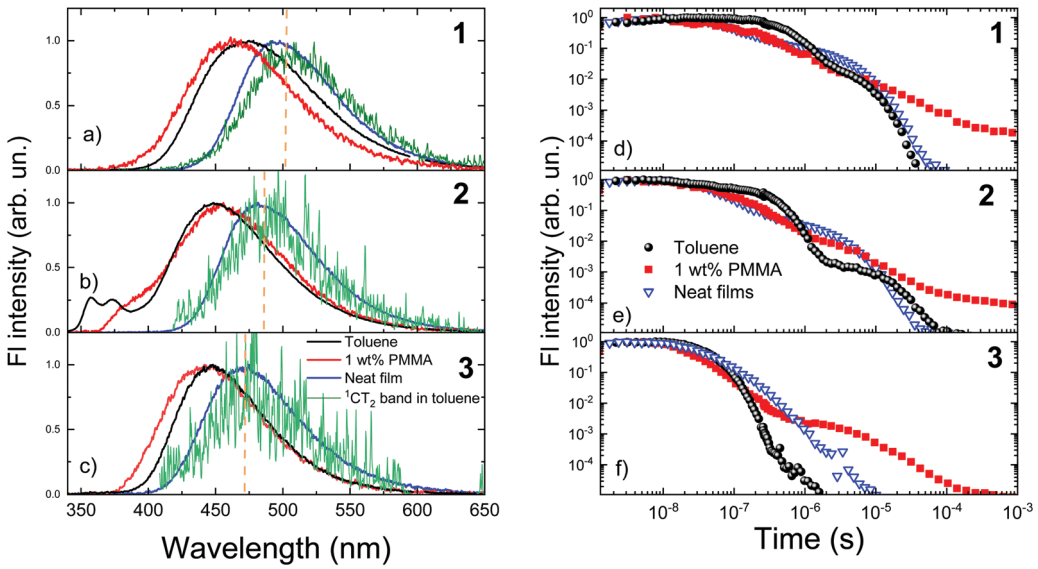

Fig. 8 (a)–(c) Normalized time-integrated fluorescence spectra of 1 wt% PMMA films (red lines), 1.2×10^{-5} M toluene solutions (black lines) and neat films (blue lines) together with fluorescence spectra of the $^1CT_2$ state in toluene solution of donor–σ–acceptor compounds **1–3** in oxygen-free conditions. Vertical lines are guides for the eye. (d)–(f) Normalized fluorescence decay transients of 1 wt% PMMA films (red figures), 1.2×10^{-5} M toluene solutions (black figures) and neat films (blue figures) of donor–σ–acceptor compounds **1–3** in oxygen-free conditions.

emission at the defect sites.[43] The fluorescence decay transients of the neat films of compounds **1–3** at the $^1CT_2$ peak are shown in Fig. 8d–f, along with the emission decay transients of the 1.2×10^{-5} M toluene solutions and 1 wt% PMMA films. A double-multiexponential decay was observed, where the initial decay of the prompt fluorescence resembled that of the 1 wt% PMMA films, while the later decay was rather similar to that of the toluene solutions (except compound **3**). For compound **3**, no clear TADF was observed. As we have already seen, the initial prompt fluorescence was strongly perturbed by conformational disorder, thus its decay was very similar to that of the 1 wt% PMMA films. The later TADF emerged only from the lowest-energy conformer states, where the higher-energy emission was quenched, therefore the TADF decay in the neat films was less perturbed by the conformational disorder and more similar to that in the toluene solutions. The fractional TADF intensity was remarkably enhanced in the neat films (except compound **3**) due to the larger number of TADF-active exciplex states. The DF/PF ratio for the neat films was 1.63 and 1.44 for compounds **1** and **2**, respectively.

The delayed fluorescence of the neat films of compounds **1** and **2** showed strong activation with temperature (see Fig. S9 in the ESI†), typical for TADF. No delayed emission was observed at 10 K, only the decay of phosphorescence after about 10 μs. For compound **3**, the enhancement of the prompt fluorescence lifetime was observed at 10 K, indicating weaker non-radiative losses at 10 K. No TADF was observed at room temperature. Probably the weak TADF observed in the toluene solutions was quenched in the neat films with efficient exciton migration towards defect sites.

Optimization of exciplex TADF

The emergence of the dominating exciplex emission is shown in Fig. 9a and b, where the fluorescence spectra of PMMA films doped with compound **1** at a concentration ranging from 1 to 100 wt% are demonstrated. The fluorescence peaked at about 460 nm at low doping concentration (0.1–2 wt%), where no intermolecular interactions were present, similarly to the emission of the $^1CT_1$ state in toluene. Some mismatch of the emission energies was due to the different polarity of toluene and PMMA (toluene is a more polar environment) and the presence of conformational disorder. The fluorescence peak started to redshift down to about 490 nm for doping concentrations of 5–30 wt% due to the emergence and later increasing number of exciplex states. Almost no further redshift of the emission spectra was observed at larger doping concentrations (30–100 wt%), where the exciplex fluorescence clearly dominated.

The transition from intramolecular TADF to intermolecular TADF from exciplex states was also observed in the fluorescence decay transients of compound **1** doped in PMMA at different concentrations (see Fig. 9c). As we can see, the fluorescence decay transients of the 1 wt% and 5 wt% doped PMMA films were rather similar, where the emission of the $^1CT_1$ states with the strong impact of conformation disorder dominates, however the rise of exciplex TADF is already observed at a 5 wt% concentration. At larger doping concentrations (*e.g.*, 10 wt%), the DF/PF ratio is enhanced (see the inset in Fig. 9) due to the emergence of the additional TADF from exciplex states.[24] The DF/PF ratio peaks at about a 20 wt% doping concentration and later starts to decrease at larger doping loads, due to the enhanced excitation mobility and subsequent quenching of the latest delayed emission at the defect sites[51] (see Fig. S10 in the ESI†). Such behavior was especially evident in the neat films. A similar trend was also observed for the TADF lifetime, which tended to decrease at larger doping concentration due to the quenching of the latest conformer states with the largest fluorescence lifetime.

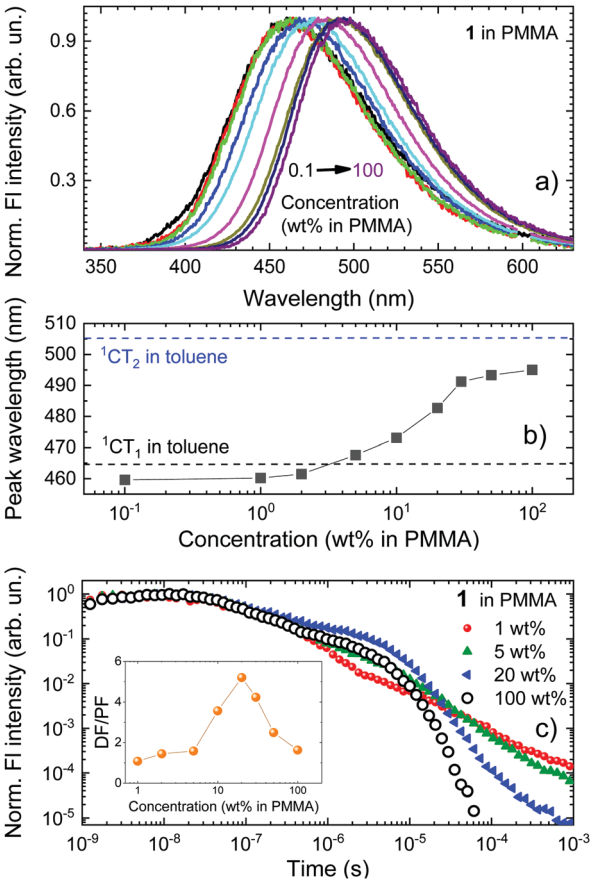

Fig. 9 (a) Normalized time-integrated fluorescence spectra of compound **1** embedded in PMMA surroundings at different concentrations. (b) Fluorescence peak wavelengths of compound **1** embedded in PMMA surroundings at different concentrations. (c) Normalized fluorescence decay transients of compound **1** in PMMA at different doping concentrations. The inset shows the DF/PF ratio at the different doping concentrations.

As we can see, intermolecular TADF is unavoidable in heavily doped polymer films, however the DF/PF ratio can be enhanced by selecting the proper doping concentration.

Conclusions

In summary, we presented a comprehensive analysis of the photophysical properties of a series of donor–σ–acceptor TADF compounds with different donor units. A hyperconjugated hexafluoroisopropylidene spacer unit was selected to reduce the electronic communication between the donor and acceptor units, seeking a negligible singlet–triplet energy gap. However, weak donor–acceptor coupling was observed, leading to remarkably prolonged fluorescence lifetimes and allowing us to observe several unusual effects. Firstly, coexisting intra- and intermolecular fluorescence of different wavelengths was observed at different time-scales even in solutions. Secondly, the initial decay with a remarkably prolonged lifetime was shown to be simple prompt intramolecular CT fluorescence, whose lifetime was shorter for the compounds with weaker electron-donating units. Interestingly, this slow initial fluorescence was susceptible to molecular oxygen. The later delayed fluorescence was shown to be TADF, originating from exciplex states, as proven by concentration and viscosity-dependent fluorescence measurements. In dilute polymer films with weakened non-radiative recombination, both prompt fluorescence and TADF were of intramolecular nature. Rather strong conformational disorder was observed due to the flexible molecular structure, leading to large temporal shifts of the emission peak. With an increasing doping load, a rise of exciplex TADF was observed, which dominated in the neat films at a similar wavelength to that in the solutions. However, the fractional intensity of TADF and its lifetime peaked at about a 20 wt% doping concentration, since the further increase of the doping load enabled excitation migration towards the defect sites and subsequent quenching of the latest TADF.

Our results have shown that weak coupling between donor and acceptor units is not favorable for efficient intramolecular TADF in σ-bridged compounds and the hyperconjugated spacer unit should be carefully designed. In-line, intermolecular interactions should be minimized in order to prevent exciplex emission in highly doped films.

Conflicts of interest

There are no conflicts of interest to declare.

Acknowledgements

SJ and ChA acknowledge funding through the EU Marie Skłodowska-Curie ITN TADFlife grant (GA. 812872). ChA also acknowledges the Japan Science and Technology Agency (JST), ERATO, Adachi Molecular Exciton Engineering Project under JST ERATO Grant Number 436 JPMJER1305, and JSPS KAKENHI Grant Number 437 17H01232.

References

1 C. W. Tang and S. A. VanSlyke, *Appl. Phys. Lett.*, 1987, **51**, 913.
2 M. A. Baldo, D. F. O'Brien, Y. You, A. Shoustikov, S. Sibley, M. E. Thompson and S. R. Forrest, *Nature*, 1998, **395**, 151–154.
3 J.-H. Jou, S. Kumar, A. Agrawal, T.-H. Li and S. Sahoo, *J. Mater. Chem. C*, 2015, **3**, 2974–3002.
4 A. Endo, K. Sato, K. Yoshimura, T. Kai, A. Kawada, H. Miyazaki and C. Adachi, *Appl. Phys. Lett.*, 2011, **98**, 083302.
5 H. Uoyama, K. Goushi, K. Shizu, H. Nomura and C. Adachi, *Nature*, 2012, **492**, 234–238.
6 R. K. Konidena and J. Y. Lee, *Chem. Rec.*, 2018, **18**, 1–20.
7 M. Y. Wong and E. Zysman-Colman, *Adv. Mater.*, 2017, **29**, 1605444.
8 T. Hatakeyama, K. Shiren, K. Nakajima, S. Nomura, S. Nakatsuka, K. Kinoshita, J. Ni, Y. Ono and T. Ikuta, *Adv. Mater.*, 2016, **28**, 2777–2781.

9 M. Mamada, K. Inada, T. Komino, W. J. Potscavage, H. Nakanotani and C. Adachi, *ACS Cent. Sci.*, 2017, **3**, 769–777.
10 Y. Xu, X. Liang, X. Zhou, P. Yuan, J. Zhou, C. Wang, B. Li, D. Hu, X. Qiao, X. Jiang, L. Liu, S. Su, D. Ma and Y. Ma, *Adv. Mater.*, 2019, **31**, 1807388.
11 F. B. Dias, T. J. Penfold and A. P. Monkman, *Methods Appl. Fluoresc.*, 2017, **5**, 012001.
12 J. Gibson, A. P. Monkman and T. J. Penfold, *ChemPhysChem*, 2016, **17**, 2956–2961.
13 M. K. Etherington, J. Gibson, H. F. Higginbotham, T. J. Penfold and A. P. Monkman, *Nat. Commun.*, 2016, **7**, 13680.
14 K. Goushi, K. Yoshida, K. Sato and C. Adachi, *Nat. Photonics*, 2012, **6**, 253–258.
15 M. Colella, P. H. Pander, D. D. S. Pereira and A. P. Monkman, *ACS Appl. Mater. Interfaces*, 2018, **10**, 793–798.
16 M. Sarma and K.-T. Wong, *ACS Appl. Mater. Interfaces*, 2018, **10**, 19279–19304.
17 D. Chen, G. Xie, X. Cai, M. Liu, Y. Cao and S.-J. Su, *Adv. Mater.*, 2016, **28**, 239–244.
18 H. Tsujimoto, D.-G. Ha, G. Markopoulos, H. S. Chae, M. A. Baldo and T. M. Swager, *J. Am. Chem. Soc.*, 2017, **139**, 4894–4900.
19 K. Kawasumi, T. Wu, T. Zhu, H. S. Chae, T. Van Voorhis, M. A. Baldo and T. M. Swager, *J. Am. Chem. Soc.*, 2015, **137**, 11908–11911.
20 S. Shao, J. Hu, X. Wang, L. Wang, X. Jing and F. Wang, *J. Am. Chem. Soc.*, 2017, **139**, 17739–17742.
21 E. Spuling, N. Sharma, I. D. W. Samuel, E. Zysman-Colman and S. Bräse, *Chem. Commun.*, 2018, **54**, 9278–9281.
22 Y.-Z. Shi, K. Wang, X. Li, G.-L. Dai, W. Liu, K. Ke, M. Zhang, S.-L. Tao, C.-J. Zheng, X.-M. Ou and X.-H. Zhang, *Angew. Chem., Int. Ed.*, 2018, **57**, 9480–9484.
23 S.-Y. Qiu, H. Xu, L. Li, H.-T. Xu, L.-K. Meng, H.-S. Pang, C. Tang, Z.-Q. Pang, J. Xiao, X. Wang, S.-H. Ye, Q.-L. Fan and W. Huang, *J. Phys. Chem. C*, 2017, **121**, 9230–9241.
24 D. Zhang, K. Suzuki, X. Song, Y. Wada, S. Kubo, L. Duan and H. Kaji, *ACS Appl. Mater. Interfaces*, 2019, **11**, 7192–7198.
25 Y. Geng, A. D'Aleo, K. Inada, L.-S. Cui, J. U. Kim, H. Nakanotani and C. Adachi, *Angew. Chem., Int. Ed.*, 2017, **52**, 16763–16767.
26 P. L. dos Santos, J. S. Ward, D. G. Congrave, A. S. Batsanov, J. Eng, J. E. Stacey, T. J. Penfold, A. P. Monkman and M. R. Bryce, *Adv. Sci.*, 2018, **5**, 1700989.
27 M. Inoue, T. Serevičius, H. Nakanotani, K. Yoshida, T. Matsushima, S. Juršėnas and C. Adachi, *Chem. Phys. Lett.*, 2016, **644**, 62–67.
28 Z. Kuang, G. He, H. Song, X. Wang, Z. Hu, H. Sun, Y. Wan, Q. Guo and A. Xia, *J. Phys. Chem. C*, 2018, **122**, 3727–3737.
29 J. C. de Mello, H. F. Wittmann and R. H. Friend, *Adv. Mater.*, 1997, **9**, 230–232.
30 C. Rothe and A. P. Monkman, *Phys. Rev. B: Condens. Matter Mater. Phys.*, 2003, **68**, 075208.
31 Y. Im, M. Kim, Y. J. Cho, J.-A. Seo, K. S. Yook and J. Y. Lee, *Chem. Mater.*, 2017, **29**, 1946–1963.
32 A. Köhler and H. Bässler, *Electronic processes in organic semiconductors: an introduction*, Wiley-VCH, Weinheim, 2015.
33 Y. Qu, P. Pander, A. Bucinskas, M. Vasylieva, Y. Tian, F. Miomandre, F. B. Dias, G. Clavier, P. Data and P. Audebert, *Chem. – Eur. J.*, 2019, **25**, 2457–2462.
34 Y. Zhang, H. Ma, S. Wang, Z. Li, K. Ye, J. Zhang, Y. Liu, Q. Peng and Y. Wang, *J. Phys. Chem. C*, 2016, **120**, 19759–19767.
35 K. L. Woon, C.-L. Yi, K.-C. Pan, M. K. Etherington, C.-C. Wu, K.-T. Wong and A. P. Monkman, *J. Phys. Chem. C*, 2019, **123**, 12400–12410.
36 M. Sarma and K.-T. Wong, *ACS Appl. Mater. Interfaces*, 2018, **10**, 19279–19304.
37 P. Valat, V. Wintgens, Y. L. Chow and J. Kossanyi, *Can. J. Chem.*, 1995, **73**, 1902–1913.
38 S. A. Boer, R. P. Cox, M. J. Beards, H. Wang, W. A. Donald, T. D. M. Bell and D. R. Turner, *Chem. Commun.*, 2019, **55**, 663–666.
39 E. V. Bichenkova, A. R. Sardarian, A. N. Wilton, P. Bonnet, R. A. Bryce and K. T. Douglas, *Org. Biomol. Chem.*, 2006, **4**, 367–378.
40 T. C. Barros, S. Brochsztain, V. G. Toscano, P. B. Filho and M. J. Politi, *J. Photochem. Photobiol., A*, 1997, **111**, 97–104.
41 T. Serevičius, T. Bučiūnas, J. Bucevičius, J. Dodonova, S. Tumkevičius, K. Kazlauskas and S. Juršėnas, *J. Mater. Chem. C*, 2018, **6**, 11128–11136.
42 T. Northey, J. Stacey and T. J. Penfold, *J. Mater. Chem. C*, 2017, **5**, 11001–11009.
43 T. Serevičius, R. Skaisgiris, J. Dodonova, L. Jagintavičius, J. Bucevičius, K. Kazlauskas, S. Jursenas and S. Tumkevicius, *Chem. Commun.*, 2019, **55**, 1975–1978.
44 M. K. Etherington, F. Franchello, J. Gibson, T. Northey, J. Santos, J. S. Ward, H. F. Higginbotham, P. Data, A. Kurowska, P. L. Dos Santos, D. R. Graves, A. S. Batsanov, F. B. Dias, M. R. Bryce, T. J. Penfold and A. P. Monkman, *Nat. Commun.*, 2017, **8**, 14987.
45 X. Zhang, M. W. Cooper, Y. Zhang, C. Fuentes-Hernandez, S. Barlow, S. R. Marder and B. Kippelen, *ACS Appl. Mater. Interfaces*, 2019, **11**, 12693–12698.
46 T. Serevičius, R. Komskis, P. Adomėnas, O. Adomėnienė, G. Kreiza, V. Jankauskas, K. Kazlauskas, A. Miasojedovas, V. Jankus, A. P. Monkman and S. Jursenas, *J. Phys. Chem. C*, 2017, **121**, 8515–8524.
47 C. F. Madigan and V. Bulović, *Phys. Rev. Lett.*, 2003, **91**, 247403.
48 B. L. Cotts, D. G. McCarthy, R. Noriega, S. B. Penwell, M. Delor, D. D. Devore, S. Mukhopadhyay, T. S. De Vries and N. S. Ginsberg, *ACS Energy Lett.*, 2017, **2**, 1526–1533.
49 Q. Zhang, D. Tsang, H. Kuwabara, Y. Hatae, B. Li, T. Takahashi, S. Y. Lee, T. Yasuda and C. Adachi, *Adv. Mater.*, 2015, **27**, 2096–2100.
50 M. K. Etherington, N. A. Kukhta, H. F. Higginbotham, A. Danos, A. N. Bismillah, D. R. Graves, P. R. McGonigal, N. Haase, A. Morherr, A. S. Batsanov, C. Pflumm, V. Bhalla, M. R. Bryce and A. P. Monkman, *J. Phys. Chem. C*, 2019, **123**, 11109–11117.
51 M. Colella, A. Danos and A. P. Monkman, *J. Phys. Chem. Lett.*, 2019, **10**, 793–798.